

Critical properties and testing methods for sealants in CCS applications

CEMENTTEGRITY Deliverable 7.2, v. 0.1
Published 2025-03-27

Author: Reinier van Noort
IFE Institute for Energy Technology, Kjeller, Norway

Review and contributions by: EBN BV, Netherlands; Astri Kvassnes (ReStone AS, Norway);
Anne Pluymakers (Delft University of Technology, Netherlands);
Benny Suryanto (Heriot Watt University, UK)

Keywords: *wellbore integrity, sealant integrity, CCS, CO₂-storage, cement testing*

Summary:

Long-term wellbore seal integrity is an important challenge for secure geological storage of CO₂. Based on experimental research performed by the CEMENTTEGRITY project, as well as literature study, we have identified three key abilities that any CCS wellbore sealant must have. These are: the ability to form and maintain a seal; the ability to resist exposure to CO₂-containing fluids; and the ability to withstand thermal shocks or cycling.

We have assessed these abilities for five different sealant compositions, using different methodologies for each ability. Based on that research, this report identifies the basic properties that are critical for ensuring a high-quality seal, as well as its long-term durability and integrity during CO₂-injection and -storage. When assessing a sealant design for a specific application, these properties and the impact of CO₂, thermal changes, and other potentially deleterious effects on them should be tested.

Furthermore, as all research groups collaborating in CEMENTTEGRITY performed their research on centrally prepared samples, we were able to compare results obtained by different research groups that used different methods to assess the key abilities. Such a comparison is presented in this report, and is used as a basis for suggesting preferred testing methods for CCS sealants.

Frequently used acronyms:

- CCS Carbon Capture and Storage
- PC Portland Cement

1. Introduction

During CO₂-injection and -storage, the annular seals behind casing or liner strings and plugs used to permanently seal injection wells, monitoring/observations wells and other (legacy) wells penetrating CO₂-storage reservoirs may be exposed to detrimental conditions that can potentially lead to a loss of seal integrity. CO₂-injection causes changes in reservoir pressure that can result in strains across the wellbore. When cold CO₂ is injected into a hot reservoir, or into a depleted hydrocarbon reservoir with low initial pressure, this can cause significant temperature and pressure changes in the injection area. If the injection is intermittent, these changes may also be cyclic [1-4].

Furthermore, sealants may be exposed to chemically aggressive fluids containing water, CO₂, and other components present in the injected CO₂ stream or the pre-existing reservoir pore fluid, including brines. The resulting mechanical, thermal, and chemical impacts can cause leakages to develop through the sealant body, along fractures through the sealant, along interfaces between sealant and wellbore or sealant and host rock, and in places where the cement was placed imperfectly [5]. Instances of such integrity concerns are underscored through multiple laboratory investigations and observations conducted on samples retrieved from wells exposed to CO₂ (e.g., [6-12]).

Wellbore sealants used to date are commonly based on Portland Cement (PC). Due to the chemical composition of PC – in particular its high calcium-content – and its brittle behaviour under stress, PC is relatively susceptible to the aforementioned mechanical, thermal, and chemical impacts. On the other hand, the carbonation of PC can also lead to sealing and healing of leakage pathways (cf. [11, 13, 14]). Therefore, new sealant materials and additives need to be developed that can better ensure long-term wellbore seal integrity for wells affected by CO₂-injection and -storage. Additionally, a more thorough understanding is needed of the limits of PC-based designs under relevant conditions.

To help address these challenges, the CEMENTTEGRITY project performed experimental research into the integrity and durability of cementitious sealant materials under conditions relevant for CCS. Note that only the hardened and cured sealant material was considered, while the properties of the slurry, such as setting time and flow behaviour, were not part of this project's scope.

Based on a literature study [15] as well as experimental and other research performed as part of the CEMENTTEGRITY project, three key abilities were identified that a cementitious material must assume upon hardening to be used successfully as a sealant in a CCS well: 1) Ability to form and maintain a seal against other materials; 2) Ability to resist exposure to chemical stressors (i.e., CO₂-containing fluids); 3) Ability to withstand physical impacts (especially thermal shock or cycling). Furthermore, the material must maintain these abilities even when exposed to any deleterious effects related to CCS. These three key abilities were discussed previously, along with key research into them by the CEMENTTEGRITY project (see also [16]). This report will focus on methods for assessing and comparing sealants with respect to the three key abilities and will also discuss the critical properties behind the key abilities and how to measure these. Finally, a Sealant Assessment Table will be presented, that can be used as a guideline when developing entirely new sealants, or when assessing and comparing different sealants for a specific application.

2. Ability to form and maintain a seal

The ability to form a seal and maintain a seal without negatively affecting the surrounding materials is the most important property of any sealant, regardless of type or application. For cementitious sealants, a seal can be formed during curing through different mechanisms (or a combination of mechanisms). For PC-based sealants, the main mechanism is the formation of physical bonds to the surrounding materials that hold the seal in place and maintain a tight interface. Alternatively, or additionally, a seal can be formed through volumetric expansion, where the curing material swells (for example through chemical reactions that lead to an increase in solid volume) to fill all open space, and even generate stress perpendicular to the sealant-steel and sealant-wallrock interfaces. Likewise, different material behaviours can be engineered to support the subsequent long-term integrity of such a seal.

Once a seal is formed successfully, it must then be maintained through subsequent changes in the chemical and physical environment to which the seal is exposed, such as changes in the stress state (as a result of pressure changes in reservoir, but also including thermally induced stress changes), and exposure to potentially chemically aggressive environments. Cementitious materials commonly used as wellbore sealants, as well as similar materials such as geopolymers, are typically brittle with low elasticity and plasticity, meaning small strains correlate to high stresses, and relatively high mechanical strengths are required to maintain integrity. On the other hand, self-healing/self-sealing mechanisms may be developed, for example based on chemical interactions between the seal and the reservoir fluids, to recover integrity when this is lost.

The importance of seal-formation and maintenance has led to the development of a number of different methodologies for measuring seal quality, or some value approximating this. However, the complexity of the subject means that no standard methodologies exist. To support the development of both effective laboratory methods for assessing and improving the seal quality of different sealants, and to enable the verification of well integrity in the field a better understanding needs to be developed.

The main methodologies used to assess seal quality for cementitious materials can be divided into two categories. Methodologies in the first category aim to assess seal quality by measuring the force needed to physically break a seal or separate a cementitious seal from steel and/or rock surfaces in contact with which it has set and cured (cf. [17, 18]). Methodologies in the second category aim to assess seal quality more directly, by measuring a pressure-driven fluid flow, i.e., leakage, along a contact surface (or contact surfaces) between a cementitious seal and components of steel and/or rock that it has been cured in contact with, or by measuring the pressure needed to induce such a flow (or flow through the material itself). For both types or methodologies, however, the results obtained may be affected by different external factors, such as the roughness, cleanness, and composition of both the sealant and the surface against which a seal is formed, and the dimensions and geometry of the test assembly. Results may also be impacted by any volumetric and temperature changes that might occur during hardening, curing, transport and storage, and testing.

In addition, CEMENTTEGRITY considered the use of electrical impedance measurements to monitor the integrity of both the seal body and the seal-steel interface, for a wellbore sealed with hydraulic sealant. For such materials, the electrical impedance measured depends on an interplay between the pore fluid composition, the pore network structure, and the interfaces at the electrodes. By comparing different electrode configurations, using either two electrodes embedded in the material, or one embedded electrode with the steel casing as the second electrode, changes in both bulk properties (due to, for example, fracturing) and interface properties (e.g., annulus formation) could be distinguished and monitored. However, due to the complexity of electrical conduction through tight

porous materials, further research is required to develop such a monitoring method, and potentially expand industry capabilities for well integrity analysis (e.g., cement bond logging).

2.1. Seal quality measurements (WP's 3 and 5)

Both types of methodologies for assessing seal quality were used during CEMENTTEGRITY, in WP's 3 (TUD) and 5 (HWU). In WP 5, bond strength was measured as the shear stress needed to push a cement plug out of a steel tube, using a patented methodology [17]. Mixed sealant S1 through S4 slurries were cured inside mild steel tubes, initially at 80°C for 3 days and 30 MPa before being raised to 150°C over 7 days and held constant at 150°C for a further 21 days. The temperature was lowered from 150°C to 20°C over a period of 7 days. When the temperature went below 100°C, the curing pressure was allowed to reach equilibrium depending on the temperature level. Before bond strength testing, the samples were pre-conditioned at 80°C (for details and results see [18-20]).

The sealant/steel samples exhibited varying bond strengths, ranging from 0.54 MPa to 4.66 MPa. The main findings are that the shear bond strengths are subject to a range of influencing factors. While compressive strength was found to be related to bond strength, high compressive strength did not guarantee good bonding performance. Upon inspection of the tested samples, it was noted that the steel casing around sealant S1 was much more corroded than those of the other samples. While this corrosion was most likely due to shrinkage of S1 during curing, the higher degree of corrosion was correlated to a relatively high bond strength, which is ascribed to the development of internal confining stress (due to the volumetric expansion associated with the formation of corrosion products at the sealant/casing interface) and the resultant rough interface, which would, in turn, increase bond strength. It was further inferred that the relatively low bond strength measured for S4 was due to its rapid initial setting and curing, which may have prevented a strong, mature bond from developing. Repeat measurements on a mix of S4 with retarder added but otherwise identical resulted in much higher bond strength (see [20]). Repeat measurements were also performed on sealant S1 cast into a stainless-steel cylinder and the same mild-steel casing in the lab environment but with induced corrosion (using electrical current), to further confirm whether corrosion of the mild steel tubing indeed caused the higher bond strengths measured initially. These measurements exhibited lower bond strength (3.56 MPa) compared to the samples with corroded mild steel (4.66 MPa), while the lab samples showed the bond strength of 0.91 MPa with no corrosion and up to 3.18 MPa with corrosion. While these repeat tests showed that corrosion can result in elevated bond strengths, corrosion alone would not explain the relatively high bond strength measured for S1. Furthermore, the increased internal confinement stress caused by corrosion should be considered non-permanent and expected to gradually disappear in the long term due to the creep and shrinkage of the sealant over time.

While seal quality as such was not the focus of the work done in WP 3 [21], seal quality was taken into account as part of the assessment of the impact of thermal shocks or cycling on seal integrity. Therefore, samples were prepared consisting of a relatively thick sheath of sealant (3 cm outer diameter, 7 cm length) cast and cured around a tube made of AISI 316L (6 mm outer diameter, 1 mm wall thickness). Seal quality was subsequently assessed on these samples by measuring annular leakage rates. This was done by applying nitrogen at elevated pressure to one end of the annular interface between seal and tube and measuring the resultant nitrogen flow along the interface. In addition, push-out measurements were also performed, where the steel tube was pushed out of the sealant sheath, in order to assess the shear stress needed to do so (i.e., a similar principle as used to measure the bond strength in WP 5 [21, 22]).

Figure 1a shows a comparison of the push-out stress before exposure to thermal cycling measured by [21, 22], against the bond strength measured by [20], i.e., in different experiments and laboratories, but with the same compositions and samples that were prepared centrally and in comparable manners. Key differences between the experimental geometries are that [20] used a plug of cement cast inside a steel tube, while [21, 22] studied a sealant sheath cast around a steel tube. Furthermore,

while the samples used by [21, 22] were much smaller than those of [20], their sealant sheath was disproportionately thick compared to the steel tube diameter. Finally, the push-out stresses and leakage rates reported in WP 3 were measured on dried samples, and the impact of drying on these measurements has not been assessed. These geometrical differences, along with differences in the temperature changes experienced by all samples between setting and testing, likely explain why only a weak correlation is observed in Figure 1c.

Figure 1b shows the annular leakage rates of S1-S5 plotted against the peak push-out stress, as measured by [21, 22]. Figure 1c similarly shows these annular leakage rates for S1-S4 plotted against the bond strength as measured by [20]. Considering these two plots, if the shear stress required to separate a cement seal from a steel tube was directly correlated to the seal quality measured as an annular leakage rate, a negative correlation would be expected. As can be seen in these graphs, even when ignoring the relatively anomalous measurements on S5, only weak, if any, correlations are obtained. Note, that while a linear correlation (least squares) is shown in both plots, any correlation between the shear strength of the interface and leakage rate is more likely to be non-linear i.e. the leakage rate is expected to increase rapidly as the shear strength diminishes and approaches zero. Furthermore, S5 was excluded from the linear correlation shown in Figure 1b. In both graphs, however, sealants S2 and S3 have relatively low leakage rates compared to the shear stress needed for separation, while S1 and S4 have relatively high leakage rates. Note that in Figure 1c, the apparent bond strength measured on the S1 sample not affected by corrosion plots closer to the shown trend line. Note also that as leakage rates were only measured on samples with stainless steel tubes, the impact of corrosion on leakage rate was not addressed.

The correlation between leakage rates and the shear stresses needed to separate a sealant sample from a steel surface shown here is relatively poor. However, the volume of data is very limited, and the impact of parameters such as sample geometry – both plug-in-tube vs. sheath-around-tube and (relative) dimensions of components – and temperature pathways undergone by the samples from curing to testing have not been addressed. Furthermore, large differences in sample geometries likely also affected measurements. As such, to ascertain if any correlation exists between the separation shear stress and interface leakage rates, and to understand how these properties may be used to determine “seal quality”, more research is required.

It is often assumed that the bond strength is correlated to the mechanical (compressive) strength of the sealant. Figure 2a shows the bond strength measured by [20], and the push-out stress measured by [21, 22] plotted against unconfined compressive strength of reference samples measured by [23] (WP 1). While a clear correlation between bond strength and UCS is not observed, a relatively good correlation to UCS is observed for the push-out stress, especially when omitting the somewhat high shear stress measured on S5. Figure 2b shows the same data plotted against tensile strength (as reported by [23] based on Brazilian disc testing). While a correlation between bond strength and tensile strength is not seen, a linear correlation is observed between the push-out stress and tensile strength, especially if S5 is omitted from consideration. Here it should be repeated, however, that the push-out stresses shown here were measured on dried samples, and with a relatively thick cement annulus surrounding a thin stainless-steel tube (6 mm contact diameter).

Interestingly, [20] reported a correlation between bond strength and setting time, particularly when the sealants are exposed to a rapid initial temperature increase (e.g., from ambient to 80°C as might occur within a wellbore at greater depths) . Based on available data, this correlation does not extend to either the pushout stress measurements or the leakage rate measurements reported by [21, 22]. However, the observed correlation does warrant further consideration, and the potential correlation between setting time and seal quality measured as leakage rate should be investigated further in future research.

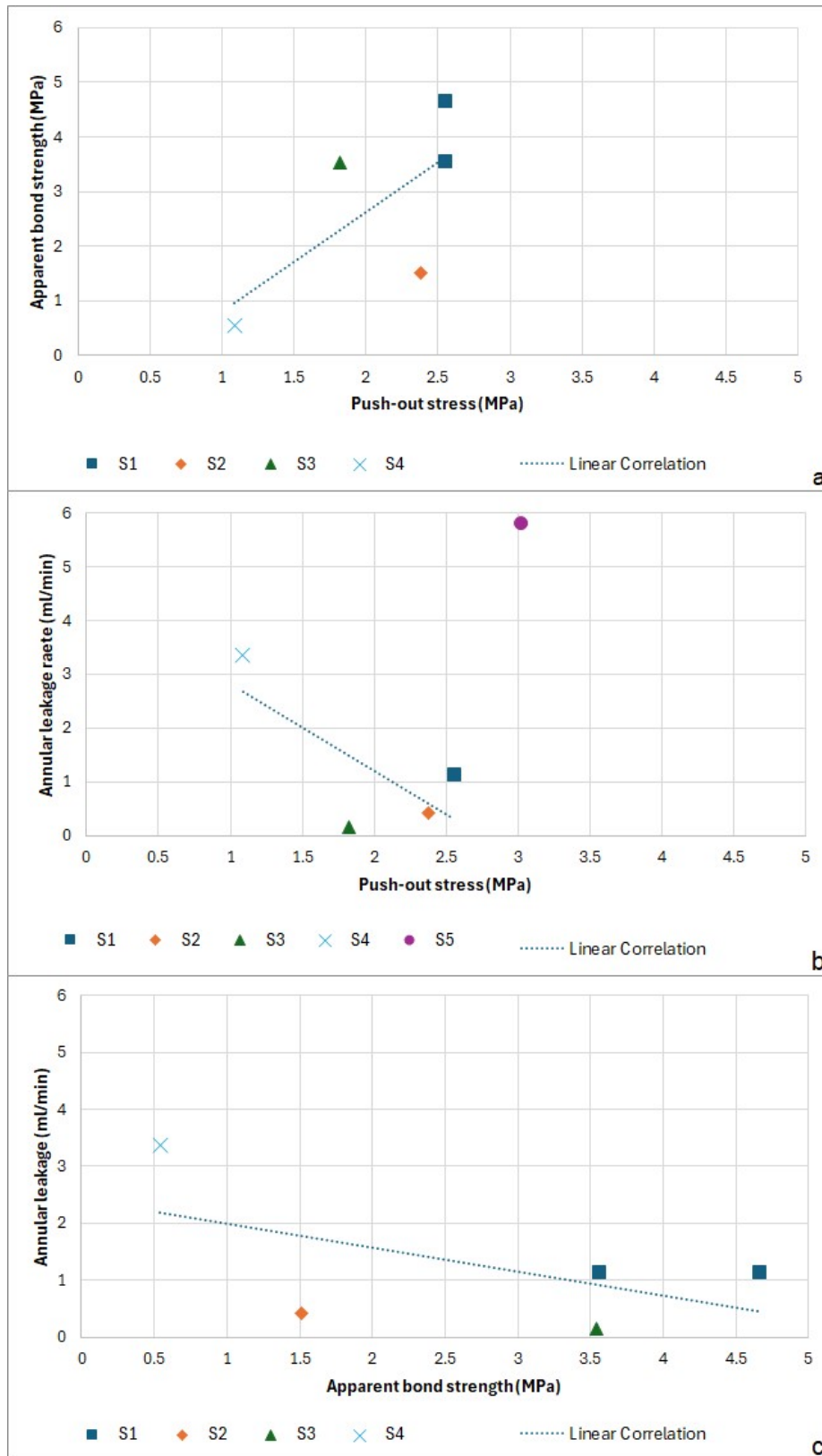
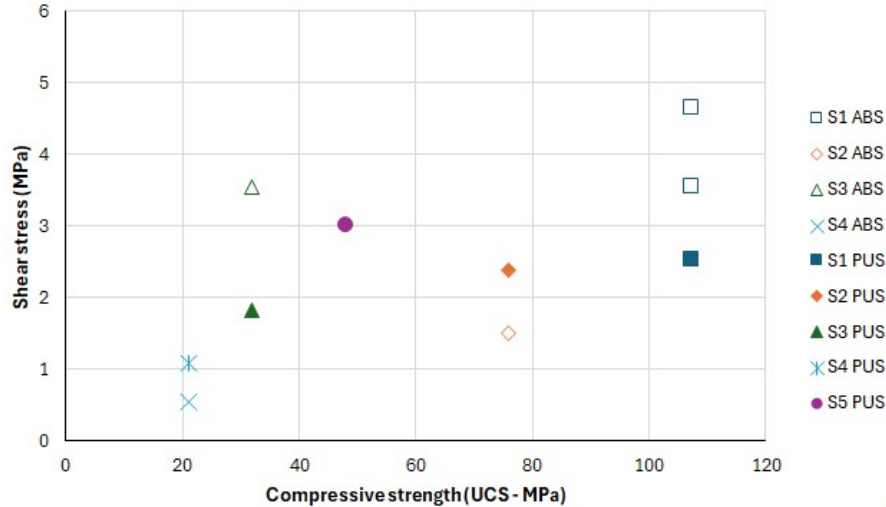
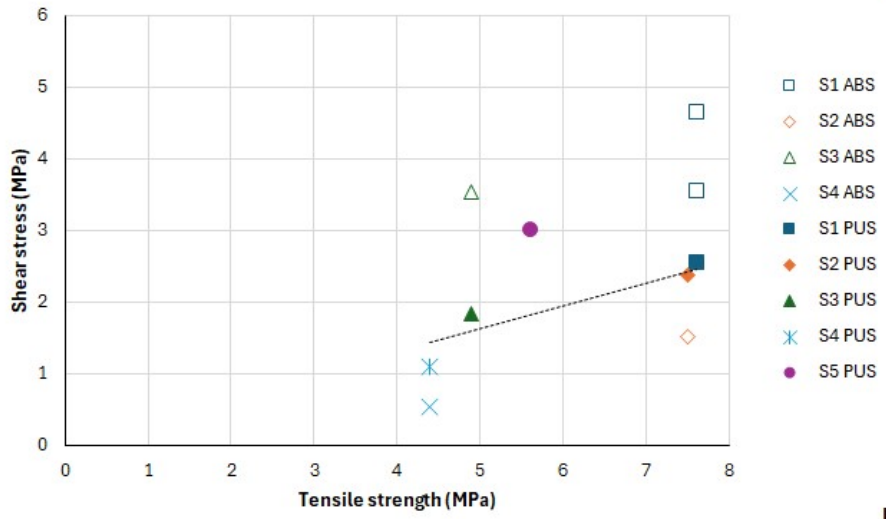


Figure 1. Plots showing: a.) apparent bond strength against push-out stress (MPa); b.) annular leakage rate (ml/min) against push-out stress (MPa), and; c.) annular leakage rate (ml/min) against apparent bond strength (MPa). Leakage rates and push-out stresses plotted here are those measured before samples were exposed to thermal cycling.



a



b

Figure 2. Graphs plotting shear stress (measured as apparent bond strength (ABS) by [18] or push-out stress (PUS) by [19, 20]) against compressive strength (a) and tensile strength (b).

2.2. Use of electrical impedance measurements to analyse and monitor seal quality

As noted, CEMENTTEGRITY studied the potential use of electrical impedance measurements to measure and monitor seal quality and the integrity of the cement-steel interface. For this purpose, two sets of samples were prepared, that either had two embedded electrodes, or one embedded electrode. For the latter samples, the steel tube surrounding the sealant sample was then used as the second electrode. A comparison (see Figure 3) between two-pin and one-pin (coaxial) impedance spectroscopy measurements should then provide insight in the sealant-steel interface contribution to the impedance signal.

The Argand diagrams presented in Figure 3 show both the real and imaginary parts of impedance, measured over a frequency range from 1Hz to 10MHz. In these plots, higher frequency measurements (the arc on the left side of the plot) result from the electrical properties of the sealant material, while the right-hand tail (part of a very large arc) results from the impedance of the electrode/material interface. Typically, the Impedance at the cusp-point between these features, where the Imaginary

Impedance is minimised, represents the direct conductivity properties of the sealant material, which should be related to the material permeability.

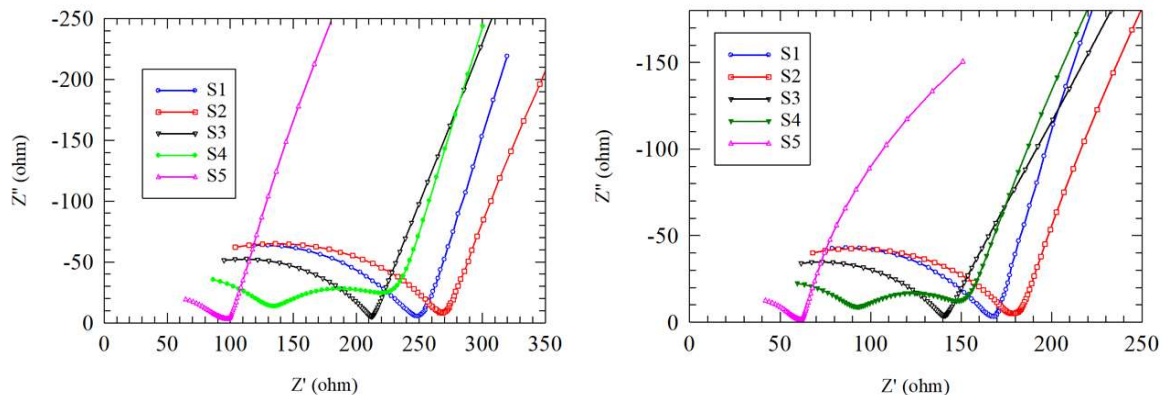


Figure 3. Argand Diagram plots of Impedance for sealants S1 to S5: a) two-pin measurements performed with two embedded electrodes vs. b) one-pin measurements made with one embedded electrode and using the steel casing as the second electrode.

Focusing now on the low-frequency tails, a comparison between sealants S1 and S3 can be used to illustrate how the obtained impedance data may be used to assess (changes in) interface conditions. Samples S1 and S3 are both based on PC as the main binder system, and are therefore very similar in (chemical) composition. However, considerable differences were observed at the sealant-steel interface during physical examination of these samples after bond strength testing with S1 samples showing extensive corrosion at this interface, which was largely absent from the S3 samples (see Figure 4). Now, to assess whether this significant difference in surface corrosion was represented in the electrical impedance data, first we need to account for the scale difference between the two different electrode configurations (2-pin twin vs. 1-pin single/casing). This can be done by normalization of these impedance measurements, by dividing each set of measurements by their respective cusp-point resistances. This allows for direct comparison of the Impedance shape characteristics on the same scale, as seen in Figure 4.

The left-hand part of the response, revealing the underlying material response, is now identical not just between the 1-pin and 2-pin measurements, as would be expected, but also for the two different sealants. However, the right-hand side of the response reveals differences between both electrode configuration and the sealant type. While the 2-pin electrode responses for both sealants have comparable trajectories, the 1-pin responses deviate from their 2-pin counterparts in contrasting ways. The S1 1-pin tail rises more steeply from the cusp-point than the S3 1-pin tail, but is also more curved. This excess curvature (in comparison to S3) is correlated to the observed corrosion at the material/casing interface. This observation thus shows the potential for using impedance measurements through the steel casing to detect alterations in the sealant/casing interface.

2.3. Recommendations for analysing seal quality

Seal quality, whether measured as a bond strength (e.g., shear force needed to separate a sealant from another material) or as a hydraulic sealability, depends on a complex interplay between different material properties of both sealant and contacting material, as well as geometry. When a bond between a sealant and the surrounding materials in the wellbore is formed, the strength of this bond could be expected to be correlated to some degree to the mechanical strength of the sealant material itself. Indeed, such a correlation is shown above for the push-out stresses as measured by [21, 22] and the unconfined compressive or tensile strengths measured on reference samples. However, other

factors may have a stronger impact on the measured bond strength, as indicated by the lack of such a correlation for the bond strength measurements performed by [20], and the relatively anomalous values measured on S5. In their tests, [20] observed that rapid initial setting during the early temperature rise (from 20°C to 80°C) exerted a negative influence on the bond strengths of S4 samples. The subsequent use of a retarding agent mitigated this problem. This suggests that optimising the early setting rate of the other sealants may also enhance their bonding properties. Another important factor may be temperature (and thus volume) changes undergone by the sample between the sample preparation and final testing. As temperature changes induce different volumetric changes in different materials, sample geometry (e.g., plug vs. sheath; as well as relative diameters and thicknesses of the different components in the sample) and size will also be important factors. Likewise, as seen in WP 5, the selection and treatment of materials other than the sealant being tested may affect the outcome. For example, corrosion on mild steel surfaces was seen to significantly enhance the measured bond strength for S1 compared to a sample cast within a stainless-steel tube. Likewise, surface roughness (from manufacturing or subsequent treatment) and cleanliness will affect the seal quality obtained, and how to best address this in testing must be considered.

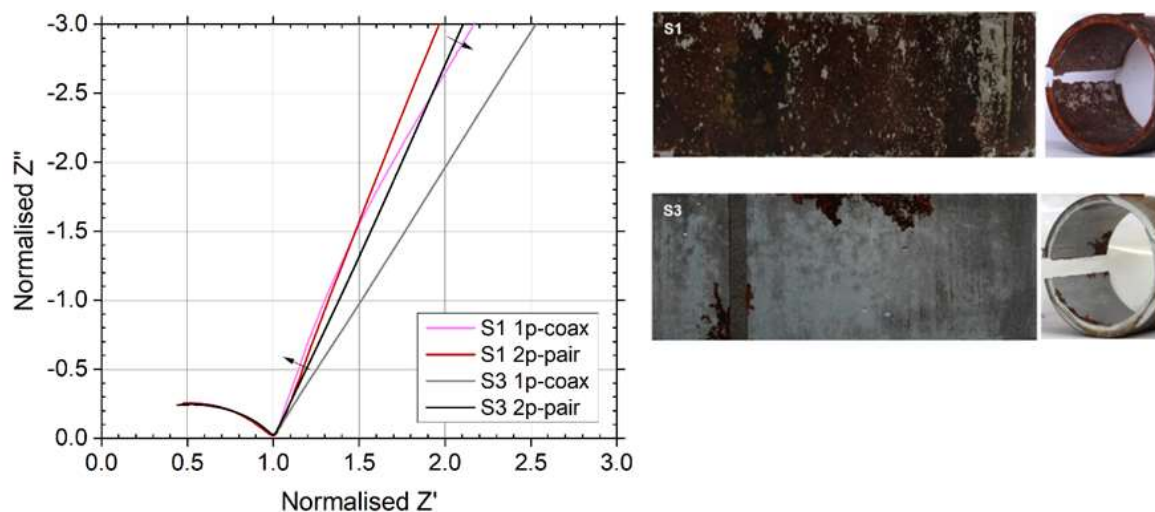


Figure 4. Argand Diagram plots of Impedance for sealants S1 and S3 with one-pin coaxial and two-pin parallel electrodes. In the one-pin configuration, measurements were taken with one embedded electrode and using the steel casing as the second electrode. The corresponding surface conditions of the sealant and inner casing are also displayed.

Directly measuring hydraulic sealability by measuring a leakage rate along a (sufficiently large) contact surface between a sealant and another material may be the most representative and relevant method to measure “seal quality”. However, such methods require relatively specialized equipment (especially when done under confinement) and are more complex and time-consuming than methods that assess seal quality as the shear stress needed to separate the interface. In the research discussed above, a weak correlation was found between the shear stress needed to separate a sealant from a contacting steel surface and the leakage rate along that interface, based on a very small number of datapoints. Further research is required, exploring the correlation between bond strength and hydraulic sealability, to investigate whether relatively rapid and simple bond strength measurements (in either plug-in-tube, or annular-seal-around-tube geometric configuration) can serve as a sufficiently representative, but relatively simple method to assess seal quality. Here, sample configuration, geometry, and dimensions, as well as external factors that may impact results should be considered to ensure representative results.

Regardless of whether a strong correlation is obtained, when more representative data is required, for example to extrapolate long-term leakage rates along annular interfaces within a well, direct measurements of leakage rates under relevant conditions will be necessary. Thus, the development and standardization of a relevant method for measuring sealability, taking into account geometry and relative dimensions while minimizing thermal changes and other factors that may unduly impact results, is essential.

Finally, electrical impedance or impedance spectroscopy measurements offer an interesting potential for not only measuring and monitoring sealant permeability and permeability in the laboratory, without disturbing or changing the sample, but also for monitoring sample properties (i.e., integrity) in the field. However, realizing those potentials will require thorough calibrations on a wide range of sealant materials and under a wide range of conditions. Furthermore, a better general understanding is required of what properties impact the electrical behaviour of materials such as sealants, to ascertain any interpretation in terms of permeability is accurate and reliable.

3. Ability to resist exposure to CO₂-containing fluids

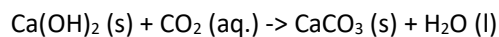
In a typical PC-based sealant, exposure to CO₂-bearing fluids (in the presence of water) initially leads to the dissolution of free Ca(OH)₂, and the precipitation of CaCO₃. During this stage, the precipitation of carbonates may lead to reductions in porosity and permeability. However, the resulting (eventual) depletion of free Ca(OH)₂ will lead to a decrease in pore water pH, and can result in the leaching of Ca from CSH-gel and even the dissolution of precipitated CaCO₃, leaving behind a degraded silica gel with (severely) compromised integrity (e.g., [8, 18]). While a sealant's ability to withstand exposure to CO₂ may be improved by reducing permeability (and porosity) to limit CO₂-ingress, considering the already low permeability of most modern sealants, it may be more effective to change the sealant's chemical and mineralogical composition, with the goal of modifying how the material reacts when exposed, and to what degree its integrity will be compromised.

The ability of a sealant to withstand CO₂ is typically assessed through laboratory testing, where samples of cured sealant are exposed to CO₂-containing fluids. This may be done in either batch set-ups, where multiple samples may be exposed simultaneously to a (static) volume of CO₂-saturated water or brine; or directly to CO₂ itself, where this CO₂ may be wet or dry; or to both simultaneously. Alternatively, samples may be exposed in a flow-through setup, where a flow of either CO₂-saturated water, or CO₂ itself (which may be wet or dry) is forced into and through a cylindrical sample by applying a pressure gradient along the sample. After exposure, a wide array of analytical methods can be used to assess the impact of CO₂, how this impact develops over time, and what other variables may affect it (see also [16]).

3.1. Testing methods for exposure to CO₂ (WP's 1 and 2)

As part of the CEMENTTEGRITY project, sealant samples have been exposed to both wet supercritical CO₂ and CO₂-saturated water, using both batch (WP 2) and flow-through (WP 1) methods. The impact of exposure was assessed using a wide range of analyses, including changes in mechanical properties, permeability, microstructure, chemical composition, and mineralogical composition. The two key aspects of the impact of exposure to CO₂ are: 1) how the material is altered, and 2) the depth to which the material is affected (especially the depth to which the material is affected negatively). This is further complicated by the fact that sealant materials exposed to CO₂-containing fluids are commonly affected by several different reactions and processes, which will have different (degrees of) impact, and may penetrate materials at different rates (or occur only sequentially).

For PC-based sealants, the main alteration upon exposure is due to the carbonation of portlandite, which can be simplified to:



As the precipitated CaCO₃ has a higher volume than the dissolved Ca(OH)₂, this reaction results in a net increase in solid volume, and will therefore typically lead to a decrease in porosity and permeability, and an increase in mechanical properties (such as compressive strength). This is also shown in WP 1, where the increase in mechanical properties is observed through a lower indentation depth in micro-indentation (i.e., hardness) measurements, and through decreased water permeabilities of all samples after exposure compared to before (except for S3 exposed to supercritical CO₂).

Figure 5 shows the depth to uncarbonated matrix for samples exposed to a forced flow of (a) supercritical CO₂, or (b) CO₂-saturated water for 180 days, plotted against water permeability after exposure, as measured by Lende et al ([23]) as part of CEMENTTEGRITY (WP 1). Note that the samples are only 80 mm long, and that as a result, some samples are fully affected within 180 days. Despite a limited number of data points, both plots show a positive correlation between carbonation depth and

(post-exposure) permeability, for both exposure conditions, suggesting that permeability does affect carbonation depth (in flow-through experiments). However, when comparing depths to uncarbonated matrix for samples exposed to a flow of CO₂-saturated water for 90 and 180 days, a linear correlation between carbonation depth and exposure duration (as would be expected if carbonation depth was controlled by pressure-driven flow through a medium of which the permeability does not change) was not obtained [23]. (Note that carbonation depths for 90 days exposure to a flow of supercritical CO₂ were not available).

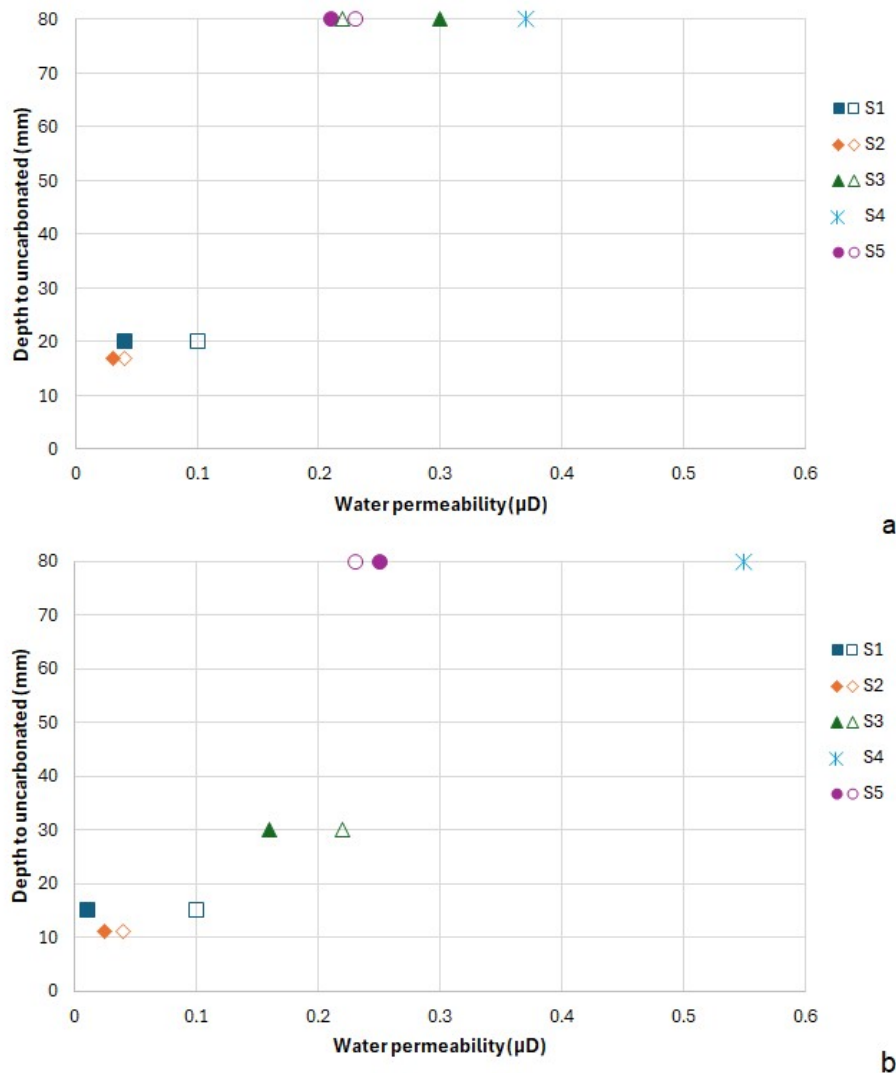


Figure 5. Depth to uncarbonated matrix plotted against the reference water permeability (sample aged for 180 days under water at pressure – open symbols) and the post-exposure water permeability, after 180 days flow-through exposure to (a) supercritical CO₂ and (b) CO₂-saturated water (closed symbols). (S4 reference permeability not shown.)

Also as part of CEMENTTEGRITY, Van Noort et al ([24]) performed batch experiments exposing sealant cylinders with a radius of 6 mm to either wet supercritical CO₂ or CO₂-saturated water. They observed that their samples were carbonated through to the centre within 28 days of exposure (i.e., carbonation depth 6 mm). However, using CT-scanning and SEM with EDS, they observed further alterations of their samples, based on microstructure (such as gel integrity) and chemical composition (in particular Ca/Si-ratio). In Figure 6 their depths to unaffected microstructure after 112 days exposure are plotted

against post-exposure permeability as measured by [23] after 180 days exposure. Note that this compares depths to unaltered microstructure and permeabilities measured at different labs, but on samples with identical compositions that were prepared and cured under the same conditions. For wet supercritical CO₂ (Figure 6a), the affected depth as assessed by [24] is largely independent of post-exposure permeability, while for exposure to CO₂-saturated water (Figure 6b), the affected depth decreases with increasing post-exposure permeability, except for S5.

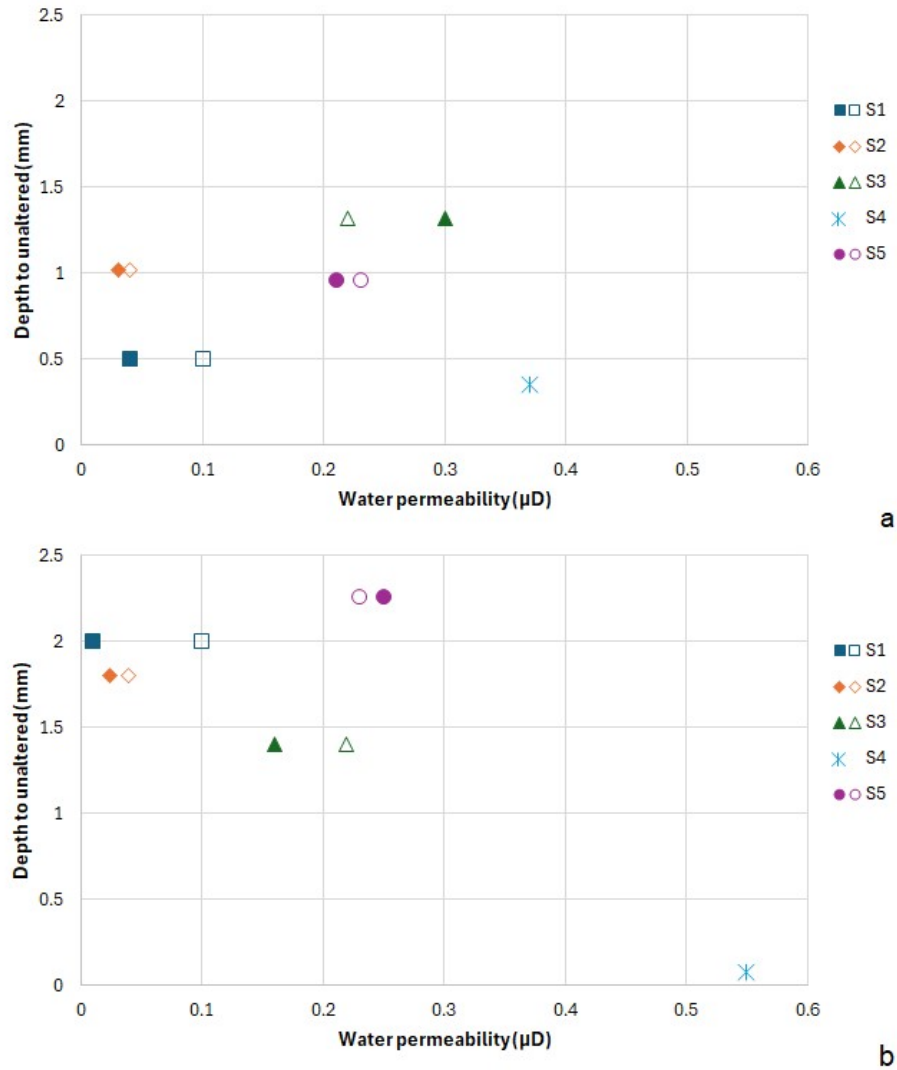


Figure 6. Depth to unaltered microstructure after batch exposure (112 days) plotted against the reference water permeability (sample aged for 180 days under water at pressure – open symbols) and the post-exposure water permeability, for exposure to (a) supercritical CO₂, and (b) CO₂-saturated water (closed symbols). (S4 reference permeability not shown.)

The correlation between carbonation depth and permeability is further investigated in Figure 7. Here, the carbonation depth as reported by WP's 1 and 2 (i.e., >6 mm after 28 days) is plotted against exposure time for sealant S1. Figure 7c presents the logarithm of carbonation depth against the logarithm of exposure duration (for the data shown in Figure 7b; i.e., exposure to CO₂-saturated water). A linear regression analysis shows a strong power-law correlation between carbonation depth (d_{carb} in mm) and exposure duration (t in days) with an exponent of 0.49 (and a constant of 1.17), giving:

$$d_{carb} = 1.17 \times t^{0.49}$$

The strong correlation observed further suggests that, for this sealant at least, permeability does not exert a strong control on the progression of the carbonation front, even if permeability does control flow through the sample. Furthermore, while a linear progression of the carbonation front with time would be expected for pressure-driven flow (through a matrix with constant permeability), the observed correlation between carbonation front and the square root of time may be indicative of a diffusion-controlled process (assuming a matrix of which the transport properties do not change). Note, though, that for diffusion-controlled transport through a porous matrix (with sufficiently low permeability), the effective diffusion coefficient, D_{eff} , is correlated with porosity and permeability via the tortuosity, with lower porosity and permeability resulting in a lower effective diffusion coefficient. Assuming a diffusion-controlled progression of the carbonation front, where:

$$d_{carb} = \sqrt{D_{eff} \times t}$$

Then, fitting the data for S1, $D_{eff} = 1.4 \times 10^{-11} \text{ m}^2/\text{s}$ is obtained (see Figure 7d). This value is comparable to, if somewhat higher than, effective diffusion coefficients of anions in tight rocks, such as shales, as reported in the literature (cf. [25-27]). Similar effective diffusion coefficients, calculated based on the same assumptions, are given in Table 1. Note that as 90-day measurements were not available for exposure to wet supercritical CO_2 , these values are based on only two data points (one of which is the minimum value of 6 mm after 28 days), and thus these values are highly speculative. For sealants S3, S4, and S5, after exposure to wet supercritical CO_2 , the progression of the carbonation front after 180 days was beyond sample dimensions, meaning a value for D_{eff} could not be calculated (but was at least $4.1 \times 10^{-10} \text{ m}^2/\text{s}$). Likewise, for S4 exposed to CO_2 -saturated water, the carbonation front after 90 days was beyond sample dimensions, meaning D_{eff} could not be calculated (but was at least $8.2 \times 10^{-10} \text{ m}^2/\text{s}$). For sample S5 exposed to CO_2 -saturated water, the sample was fully carbonated after 180 days, meaning the estimated D_{eff} value given here should be considered a minimum.

It is interesting to compare these extrapolations to other such extrapolations reported in the literature. Based on experiments carried out by Kutchko et al [8, 10], Brunet et al. [28] suggest that the ratio between the volume of free $\text{Ca}(\text{OH})_2$ and porosity has a strong control over the depth of carbonation, and the associated impact of CO_2 -exposure, where for ratios higher than 1, CO_2 -exposure leads to a narrow, sharp carbonation front penetrating less deep into the sample, but also more significant degradation behind this carbonation front, while for lower ratios, carbonation penetrates more deeply into the sample but also results in less degradation. When considering our results for S1 and S2, the extrapolations above show a deeper carbonation depth for S1 (with relatively high free $\text{Ca}(\text{OH})_2$ -content, but also higher porosity), but also show considerably less degradation behind the carbonation front for S2 (which has a lower free $\text{Ca}(\text{OH})_2$ -content due to the addition of silica fume) than for S1. Note that the samples that the model by Brunet et al. is based on were quite different in composition to the samples studied here, which may explain some of the discrepancies.

The above correlations between carbonation depth and time suggest that carbonation progression is more likely controlled by diffusion than by pressure-driven flow, even in the forced-flow experiments with exaggerated pressure gradient. This suggests that batch testing, with fluid replacement to limit changes in the exposure fluid composition that would otherwise slow down chemical interactions between fluid and sealant, may be more relevant than flow-through testing for assessing the progression of a carbonation front with time, except perhaps for samples with very high permeability.

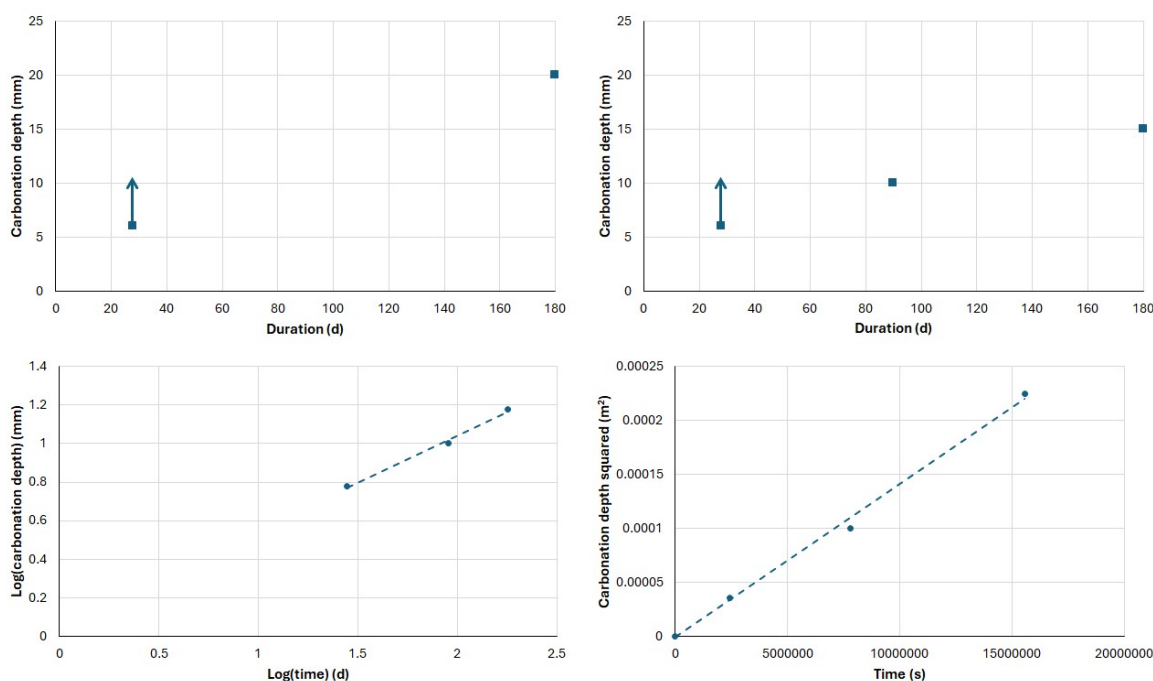


Figure 7. Plots correlating carbonation depth (mm) to exposure duration (in days – d) for batch (WP 2) and flow-through (WP 1) exposures of S1 samples. a) Exposure to wet supercritical CO₂; b) exposure to CO₂-saturated water; c) log-log plot of the data shown in b; d) square of carbonation depth (m²) after exposure to CO₂-saturated water plotted against exposure time (s).

Based on equilibrium calculations using the OLI-studio software, the CO₂-content in a stream of CO₂-saturated water at 20°C and 6.2 MPa is relatively low (~1.31 mol/l). For sealant S1, based on a porosity of 35.6 % (as measured by Li and Plumakers using a He-pycnometer) this means that the CO₂-content in one pore volume of CO₂-saturated water prepared and injected at room temperature (0.47 mol CO₂ per l of sealant, ignoring volumetric expansion due to temperature increase and CO₂-exsolution) is far from sufficient to carbonate all Ca in one volume of sample (~ 17 mol Ca per l of sample, based on XRF-analysis, but note that the free Ca(OH)₂-content may be as low as 0.56 mol per l of sample, as determined by extraction with ethylene glycol and subsequent analysis with ICP-MS). Thus, while the injected hydrous fluid may flow into and through the sample relatively quickly, its CO₂-content will be depleted at a relatively shallow level by reaction with dissolving Ca, and as a result the carbonation front will advance more slowly than the flowing fluid. Furthermore, as the injection of CO₂-saturated fresh water will induce dissolution and leaching, this is expected to result in a downstream displacement of Ca (and other soluble elements). Similarly, when injecting supercritical CO₂, the molar density of CO₂ (6.1 mol/l for wet CO₂ at 11.7 MPa and 80°C) is considerably lower (2.2 mol CO₂ per l of sample) than required for carbonating all Ca.

Figure 8 shows SEM cross-sections of samples of sealant S1 exposed to a flow of CO₂-saturated water for 180 days (a and b), or a static volume of CO₂-saturated water for 112 days (c). Figure 9 shows SEM cross-sections of samples of sealant S1 exposed to a flow of wet supercritical CO₂ for 180 days (a and b), or a static volume of wet supercritical CO₂ for 112 days (c). Curves underneath the SEM images show Ca/Si-ratios measured along the sections.

Table 1. Extrapolated effective diffusion coefficients (D_{eff} in m^2/s) for carbonation depth in cementitious sealants at 80°C and pressures ranging from 6 to 12 MPa, based on data from batch exposures by Van Noort et al (WP 2 – [29]) and flow-through exposures by Lende et al (WP 1 – [23]).

Sealant	Exposure media	D_{eff} (m^2/s)	Carbonation depth after 30 years (mm)
S1	CO ₂ -saturated water	1.4×10^{-11}	116
	Wet supercritical CO ₂	2.5×10^{-11}	155
S2	CO ₂ -saturated water	0.8×10^{-11}	87
	Wet supercritical CO ₂	1.8×10^{-11}	132
S3	CO ₂ -saturated water	5.7×10^{-11}	232
S5	CO ₂ -saturated water	4.5×10^{-11}	656

Figure 8a shows the carbonation front resulting from exposure to a flow of CO₂-saturated water. This front was observed at about 12 mm from the injection site. At the front, a roughly ~70-100 μm wide zone is observed, where the sample porosity is reduced to near-zero due to dense carbonate precipitation. Within this zone, the Ca/Si-ratio is elevated considerably. Ahead of this front, the cement matrix appears unaffected, though over the full mm shown, the Ca/Si-ratio is somewhat lower than the reference value measured on the same sample several mm away from the carbonation front. Behind the front, the carbonated sample has a much coarser, higher porosity. Here, from about 100-150 μm behind the carbonation front, the Ca/Si-ratio is approximately equal to the reference value over the section shown.

Figure 8b shows a cross-section inwards from the end-face through which CO₂-saturated water was injected. Here, a leached outer zone is observed of about 1100-1200 μm wide, where the Ca/Si-ratio is strongly depleted, and this has resulted in a degraded (dark) microstructure. At about 1150 μm from the sample surface, the Ca/Si-ratio increases sharply to reference values, and a porous, carbonated microstructure is established. In the outer 200-300 μm of the sample, some irregular precipitation, assumed to be calcite, is observed, and this corresponds to a gradual, minor increase in Ca/Si-ratio.

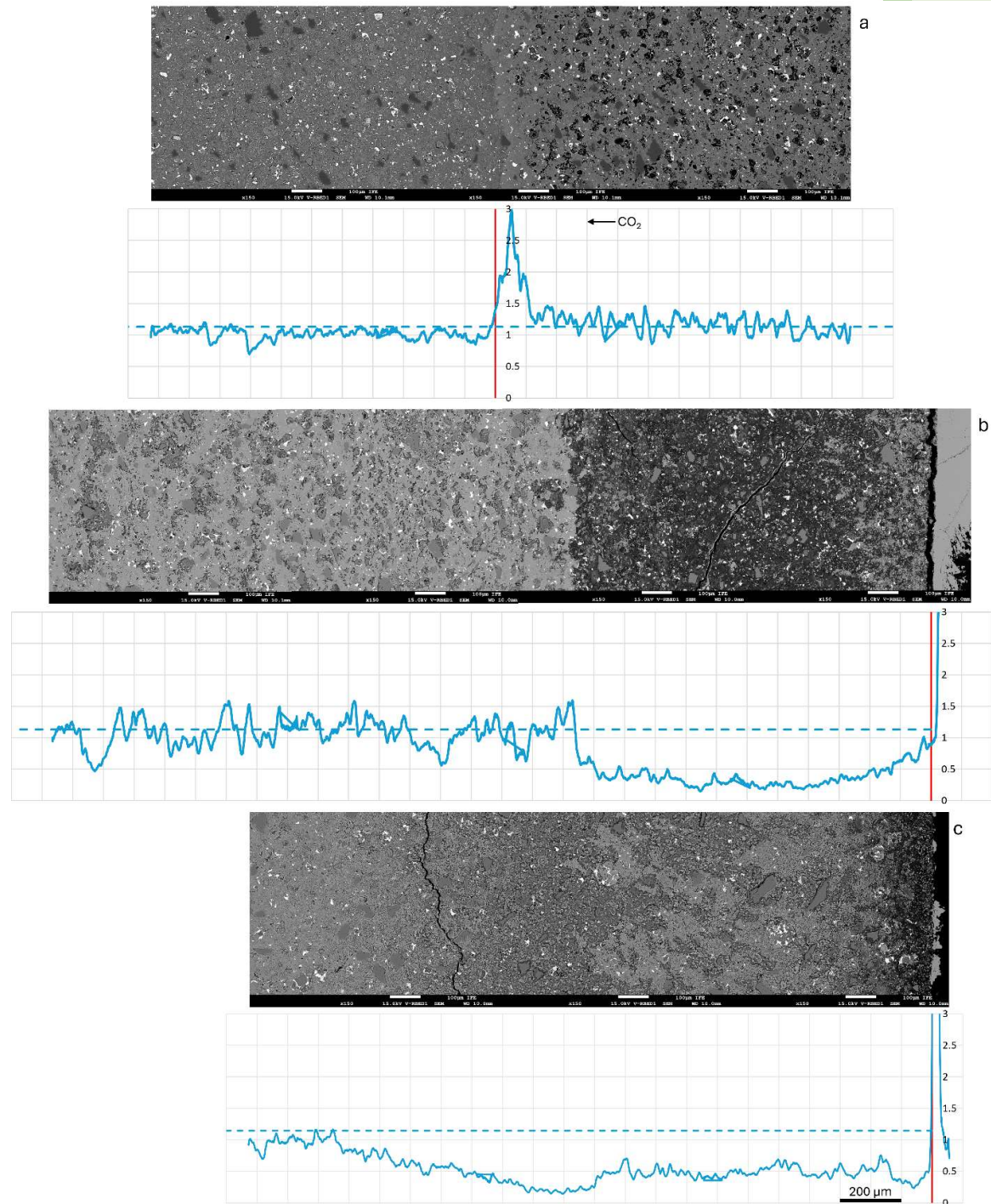


Figure 8. Composite SEM micrographs using backscatter electron imaging, showing cross-sections of samples of sealant S1 exposed to a flow of CO₂-saturated water for 180 days (a and b), or a static volume of CO₂-saturated water for 112 days (c). The carbonation front is shown in (a), while (b) and (c) show the sample surface. The curves underneath the images show the Ca/Si molar ratios measured along the SEM micrograph. Magnification 150x; scalebars and vertical gridline spacing are 100 μm. The y-axes range from 0 to 3. Dotted lines show the reference Ca/Si-ratio of 1.15, measured near the centre of an unexposed sample.

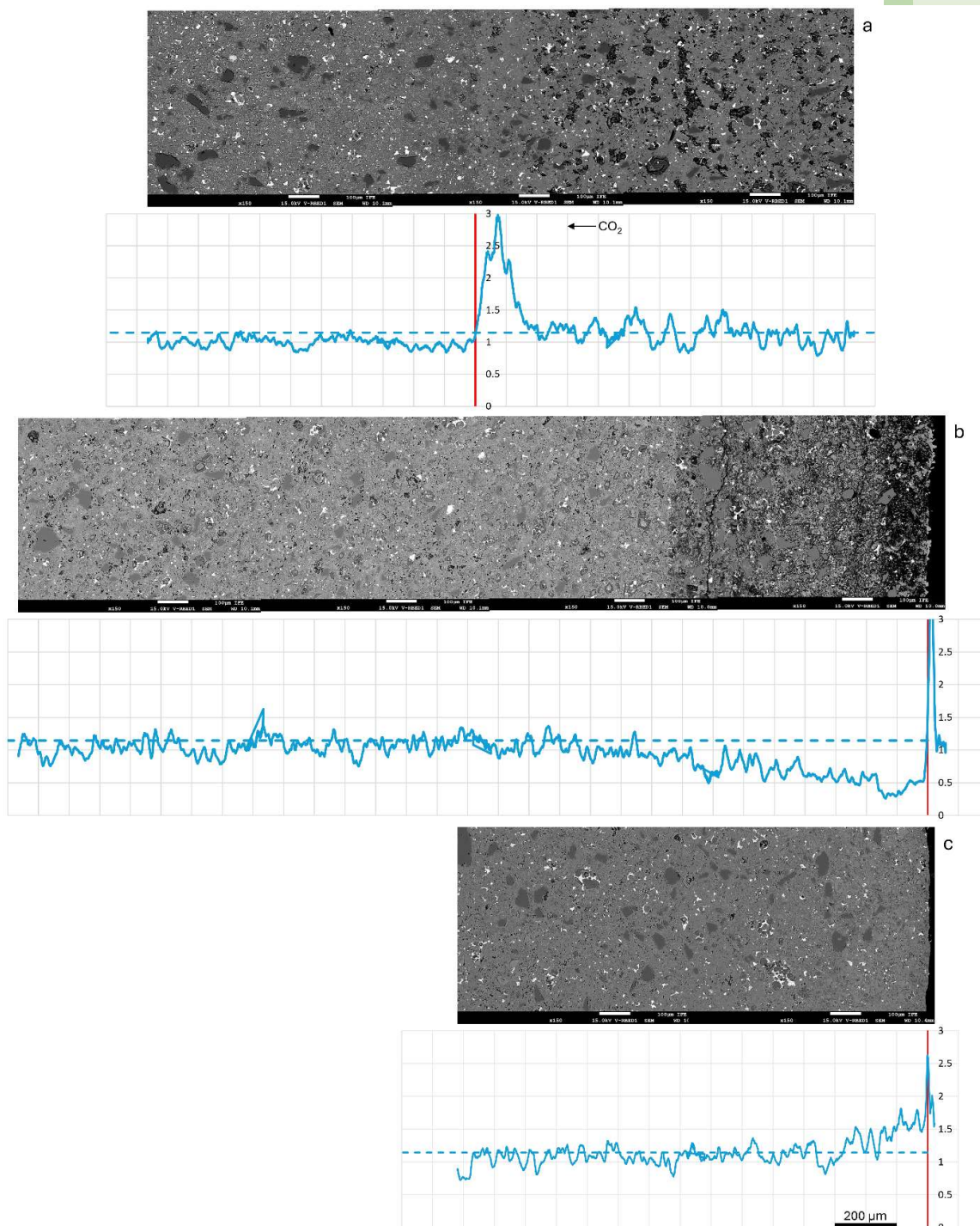


Figure 9. Composite SEM micrographs using backscatter electron imaging, showing cross-sections of samples of sealant S1 exposed to a flow of wet supercritical CO₂ for 180 days (a and b), or a static volume of wet supercritical CO₂ for 112 days (c). The carbonation front is shown in (a), while (b) and (c) show the sample surface. The curves underneath the images show the Ca/Si molar ratios measured along the SEM micrograph. Magnification 150x; scalebars and vertical gridline spacing are 100 μm. The y-axes range from 0 to 3. Dotted lines show the reference Ca/Si-ratio of 1.15, measured near the centre of an unexposed sample.

These microstructures are comparable to those observed in the batch-exposed sample shown in Figure 8c. Here, a strongly depleted outer zone of about 150-200 μm (with severely depleted Ca/Si-ratio) surrounds a zone where a solid product, again assumed to be calcite, has precipitated irregularly

within a depleted and degraded matrix with coarse microstructure. Where this precipitate is observed, the Ca/Si-ratio is somewhat elevated, though still depleted with respect to reference values. Inwards of this, a rough, depleted zone with strongly reduced Ca/Si-ratio is observed, which is comparable to the depleted zone seen in Figure 8b. However, whereas in Figure 8b, the Ca/Si-ratio increases sharply (and the microstructure also changes sharply), in Figure 8c, the Ca/Si-ratio (and microstructure) change much more gradually. Furthermore, depletion is observed considerably more deeply into the sample. The stronger depletion observed in the batch-exposed sample can most likely be ascribed to its exposure to a relatively large external volume of water, leading to significant dissolution followed by the removal of solutes from the sample. This would also explain the strongly degraded outer 150-200 μm of this sample.

Figure 9a shows the carbonation front resulting from exposure to a flow of wet supercritical CO_2 . Similar to the front in the sample exposed to CO_2 -saturated water, a zone with strongly reduced porosity due to carbonate precipitation is observed behind the front, though here this zone is somewhat wider, at about 150 μm wide. It is similarly associated with a strongly increased Ca/Si-ratio, while ahead of the front this ratio is somewhat depleted. From about 150-200 μm behind the front, the Ca/Si-ratio in the carbonated zone is similar to the reference value. Here, porosity is elevated compared to the carbonation front, and the carbonated microstructure is relatively coarse.

Figure 9b shows a cross-section inwards from the end-face through which wet supercritical CO_2 was injected. Here, an outer zone of about 150-200 μm wide has a degraded appearance, and a strongly depleted Ca/Si-ratio. Further inwards, the Ca/Si-ratio increases somewhat, and the microstructure appears less degraded, most likely due to precipitation of carbonates (assumed to be calcite) within the leached Si-gel matrix. At about 800-850 μm from the sample surface, the microstructure transitions quite sharply to a more regular carbonated matrix, while between 800 and 900 μm from the sample surface, the Ca/Si-ratio increases relatively gradually to (approximately) reference values.

This microstructure is quite different from that observed in the batch-exposed sample, shown in Figure 9c. Here, exposure led to a somewhat increased density near the sample surface, with elevated Ca/Si-ratio in the outer ~ 300 μm . A potential cause for this difference could be the presence of some liquid water in the CO_2 -stream in the flow-through experiments, or the advective displacement of pore water by injected CO_2 , leading to downstream (i.e., inwards) transport of dissolved Ca. Note that some (minor) degradation (and Ca-depletion) was observed in the outer ~ 150 μm of S1 samples exposed in batch tests for 4 or 8 weeks.

In addition, WP 2 studied how the presence of impurities in injected CO_2 may affect how exposure to this CO_2 impacts sealants. Van Noort et al ([29]) performed experiments with 1.6 mol% H_2S in the CO_2 -phase, and with a CO_2 -phase in equilibrium with concentrated sulfuric acid. Overall, the impact of these impurities was relatively minor, with their presence mostly enhancing the effects of CO_2 -exposure, especially in more reactive sealants (such as S1), while also leading to reduced carbonate precipitation. The strongest impact was observed for exposure to CO_2 -saturated water with H_2S , where (in particular for sealant S1), H_2S enhanced leaching, and resulted in reduced CaCO_3 precipitation. However, while the impact of impurities reported here for sealants based on cementitious materials, and especially for exposure to a supercritical CO_2 -phase, was minor, impurities should not be neglected completely, especially when considering the relative volume of a seal compared to the volume of injected CO_2 . In addition, the reduced carbonate precipitation observed in these tests implies that these impurities may negatively affect a (PC-based) sealant's self-sealing capability. Impurities should also be considered when developing new sealant materials that may be more vulnerable to specific impurities. Furthermore, some impurities may have a stronger impact under different PT-conditions. For example, the presence SO_x can lead to the formation of CaSO_4 as either gypsum or anhydrite depending on temperature, and this may have a strong impact on sealant porosity and permeability.

3.2. Recommendations for CO₂-exposure

Based on the discussion above, the progression of a carbonation front appears not to be controlled by pressure-driven flow. Instead, front progression shows a time-dependence implying diffusion-control. Furthermore, even when applying an unrealistically high pressure gradient, full carbonation (i.e., progression of the carbonation front along the full sample length of 80 mm) was not achieved in many of the sample tested, and exposure commonly resulted in multiple different reaction zones with varying properties. Therefore, when considering the progression of carbonation through (PC-based) sealant samples, and the impact of carbonation on sealant (mechanical) properties, the use of testing methods that can measure relevant properties locally rather than on a sample scale, such as micro-indentation methods for mechanical properties, will be beneficial to obtain accurate properties for altered materials. In addition, when carrying out exposure, exposure methods based on forcing a flow through a sample cylinder are relatively complex, and more likely to be affected by technical incidents, such as pump failure. Furthermore, depending on the application for which a sealant material is tested, flow-through exposure may be less representative than batch exposure in many cases.

In addition, the impact of CO₂-exposure was very different depending on whether a sealant was exposed to CO₂-saturated water or wet supercritical CO₂, with the former leading to significant leaching as dissolved Ca (and other cations) diffused out of the sample and into the exposure fluid. This should be considered when testing new sealants, or when assessing sealants for a specific application or well, as samples should be exposed under relevant conditions, to the relevant fluids expected in-situ, to ensure representative results are obtained.

4. Ability to withstand thermal shocks or cycling

Injection of relatively cold CO₂, along with large pressure drops during CO₂-injection, especially when injecting into depleted hydrocarbon (gas) reservoirs with very low pore pressure, can lead to sharp temperature gradients. If injection is periodic, this can also lead to temperature cycling. Therefore, sealants used in CCS must be able to withstand such (repeated) thermal shocks and maintain seal integrity as part of the wellbore-sealant-caprock system.

Considering the bulk sealant itself, the thermally induced stress experienced by a sealant exposed to a given thermal shock is inversely correlated to its thermal diffusivity ($a = \lambda/\rho c$, where λ is the thermal conductivity, ρ is the bulk density, and c is the specific heat capacity). In addition, a low thermal expansion coefficient (α) and low Young's modulus (E) will also lead to lower thermal stresses. Cracking (and consequently loss of seal integrity) results when the thermally induced stress exceeds the material's tensile strength plus the effective confining pressure. Hence, along with low α and low E , a high a (i.e., high λ and low c), and a high tensile strength will improve a sealant's ability to withstand thermal shock. However, it is at least equally important to consider the sealant as part of the wellbore system, as annular leakage pathways may also form between sealant and steel wellbore (or sealant and caprock). Here, thermal stresses may be minimized by engineering the sealant material to have a thermal expansion coefficient that is as similar as possible to the expansion coefficients of the steel and rock that the sealant is in contact with.[21, 30]

Testing in CEMENTTEGRITY (cf. [21]) has shown that thermal shocks may result in cracking of sealants, but that placing samples under confinement helped prevent such damage for all sealants tested. However, the formation of leakage pathways along the annular sealant-casing or sealant-rock interfaces along the sealant interfaces is a more likely mechanism leading to the loss of wellbore integrity. This was tested by measuring a leakage rate along an annular contact between an inner steel tube and a surrounding sealant sheath before and after thermal shocks induced by periodically flowing cold water through the steel tube while the sample was heated.

4.1. Recommendations for assessing thermal impacts

Wellbore seal systems are most vulnerable at their interfaces, where differences in material properties may lead to stress generation and concentration, while mechanical strengths may be lower. Thus, when considering thermal cycling or shocks, annular leakage formation and development is more likely than cracking of the sealant body itself. Accordingly, when testing sealants against thermal shocks or cycling, assessing the development of leakages along interfaces is more relevant than testing the sealant itself. Furthermore, as confinement has been shown to have a strong preventive effect on leakage formation due to thermal effects, confinement should be taken into account in testing as well. However, testing without confinement is much less complex, with more limited technological requirements. As such testing without confinement is more extreme, it may also give a clearer distinction between different materials and may thus be more useful when comparing and ranking different sealants. More complex testing under confinement may then be used on selected materials, to obtain more accurate understanding required for modelling and extrapolation beyond the laboratory.

In addition, research by Li and Pluymakers (e.g., [21, 30]) has shown good correlation between key thermal properties, such as thermal expansion coefficient and thermal conductivity, and the impact of thermal cycling or shocks. Therefore, at least for initial assessments, measurements of these properties may be used to qualify different materials. These thermal properties and how they affect integrity when seals are exposed to thermal changes should also be considered when performing numerical modelling on sealant integrity.

As thermal shocks or cycles have been shown to affect mechanical properties and permeability, it may also affect a material's ability to withstand CO₂-containing fluids. This aspect has not been studied here but should be addressed in future work. Likewise, the impact of CO₂-exposure on thermal

properties of wet samples, and thus the ability of a wet sealant (that may dry out and react over time) to withstand exposure to thermal shocks or cycling, has not been addressed. As carbonate precipitation strongly affects both the microstructure and the mineral composition of the affected sealant, it could have a significant impact on its thermal behaviour as well.

5. Critical Sealant Properties

Based on the three Key Abilities, as well as properties identified by regulatory documents ([31-34] – see also [15]), several critical properties have been identified that should be tested when assessing sealants. Furthermore, the impact on these properties of exposure to CO₂-containing fluids, thermal shocks or cycling, as well as other potential mechanisms that may negatively impact seal integrity in the geological storage operation under consideration should also be determined, to ensure these critical properties are not unduly affected. The critical properties are listed in Table 2.

Table 2. Critical properties for cementitious sealants to be used in wells exposed to CO₂ (as part of CCS).

Permeability	
	Low permeability required; Further reducing permeability may improve ability to withstand CO ₂ -exposure.
Mechanical properties	
- Compressive strength	Sufficiently high
- Tensile strength	High
- E-modulus	Low
- Poisson’s ratio	Suitable (0.1-0.3)
- E/C-ratio	Low
Volumetric behaviour	
- During curing	No shrinkage; Expansion preferred.
- Over time	No shrinkage; Expansion preferred.
Thermal properties	
- Thermal diffusivity	High
- Thermal expansion coefficient	Suitable (i.e., similar to surrounding materials)
Mass	
	Mass changes from exposure indicate ongoing reactions that may cause (or lead to) degradation.
Composition	
- Chemical, - Mineralogical, - Microstructure.	Chemical, mineralogical, and microstructural changes should be assessed to determine the depth to which the material is affected by various changes, and to what degree these changes are deleterious to the material’s integrity as a sealant.

5.1. Permeability

The permeability of a porous material is typically determined by measuring fluid flow through a sample when imposing a pressure gradient. Permeability can be measured by establishing a constant flow through a sample at room temperature, and with one side of the sample at atmospheric pressure (typically fully open to the atmosphere), as described in API 10B-2 [35]. However, a more representative result may be obtained when permeability is measured at elevated temperature and downstream and confinement pressures, comparable to those expected in-situ. Testing at elevated temperature has the additional benefit of lower fluid viscosities, which lead to higher flow rates and thus higher measurement accuracy and (potentially) shorter test durations. Furthermore, carrying out permeability measurements using the actual fluids to which sealants are expected to be exposed (e.g., water or brine, CO₂, or CH₄) may yield more representative measurements. Using water (or another

liquid) also eliminates the Klinkenberg effect that affects measurements carried out using gas. When comparing permeabilities before and after exposure to CO₂, thermal cycles, or other deleterious mechanisms, care must be taken to perform such permeability measurements at similar PT-conditions and using the same fluid, to eliminate any potential artefacts. (For further discussion, see [15].)

Finally, when a flow-through method is used to expose a sealant sample to CO₂-saturated water or CO₂ itself, accurate tracking of flowrates along with up- and downstream pressures (or either pressure and the differential pressure between them) and temperature can allow in-time tracking of overall sample permeability, and permeability changes. However, as chemical interactions during exposure may affect the chemical composition of the flowing stream, measurement of pre- and post-exposure permeabilities, for example using clean water, may help pinpoint accurate values.

5.1.2 Using electrical impedance measurements to assess permeability

CEMENTTEGRITY has explored the use of electrical impedance measurements as an alternative method for assessing sealant permeability. Using a method based on electrical conduction has the added benefits that the use of such methods does not affect the material or pore fluid, and that such methods could be adapted for in-situ monitoring of seal integrity. When an (alternating) electrical current is applied to a non-conducting, porous material such as a rock or a hydraulic sealant material like those considered by CEMENTTEGRITY, the electrical impedance response will be influenced by the material pore network (via direct ionic conduction and polarisation) as well as the material-electrode interfaces. In CEMENTTEGRITY, we studied the electrical impedance response for two different types of electrode configurations, either using two separate electrodes (to measure bulk sealant properties), or using one electrode and the steel casing (to measure interface properties at this casing). When considering the former configuration, and assuming ionic conduction in the bulk pore fluid to constitute the main conduction mechanism, the bulk electrical conductivity measured should correlate with the sealant permeability (especially the water permeability). However, it should be stressed that the conductivity of the pore water will also strongly affect the bulk conductivity.

To consider this possible correlation between the (water) permeability of a sealant and its electrical conductivity, first conductivity (or its reciprocal resistivity) values need to be derived from the complex, frequency dependent responses obtained (as shown in Figure 3). The frequency range of measurements (which increase from right-to-left on the plots) was 1Hz to 10MHz. Except for S4, all materials show the typical response expected for ionic conduction through a porous material. For these materials, the conductivity of the sealant material can be derived from the real impedance (Z') at the frequency where the imaginary impedance (Z'') is minimal. S4 shows a more complex frequency-dependent behaviour that resembles the response of materials containing isolated conductive inclusions.

Figure 10 presents the conductivity data derived from the impedance data presented in Figure 3, plotted against water permeability measurements of unexposed reference samples measured in WP 1. For the three sealants based on PC, pore fluid compositions should be assumed similar enough that a direct comparison can be made, while for S5, the pore fluid ionic strength is expected to be considerably higher due to the activators used in this material. For S4, the pore fluid composition may also be different. Furthermore, due to the more complex frequency-dependent behaviour of this material, an accurate real impedance (and thus conductivity) cannot be estimated based on the data available.

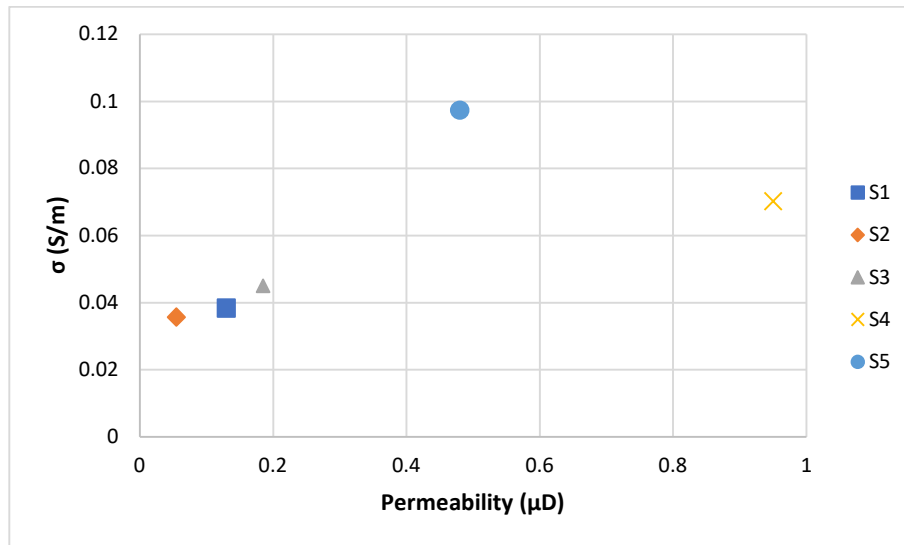


Figure 10. Conductivity (σ , in S/m) plotted against water permeability of unexposed reference samples (in μD).

Overall, Figure 10 shows an increasing conductivity with increasing permeability, as would be expected. S4 exhibits a relatively low conductivity compared to its permeability, possibly due to a lower ionic strength in the pore fluid. By contrast, S5 has relatively high conductivity compared to its permeability, suggesting that its pore-fluid conductivity may be higher than that of the PC-based materials S1-S3.

Based on the data presented here, electrical impedance measurements may provide a way to assess seal permeability, once other properties that affect electrical impedance measurements, such as pore fluid composition, can be taken into account. However, this would require thorough calibrations based on a much wider range of different samples. Our results also suggest that it should be possible to monitor the integrity of a seal in-situ using electrical impedance monitoring, as sudden changes in material integrity (i.e., fracturing) should lead to measurable changes in impedance. This should be investigated further through additional testing, for example, by monitoring the impedance (or conductivity) of a wet sealant sample under load while it fractures, and by testing samples with varying moisture contents. The development of an extensive database comprising a variety of sealant compositions and types will be required for employing this method to detect changes in sealant integrity.

5.2. Mechanical properties

As discussed in [15], standard unconfined and confined methods exist for measuring the relevant mechanical properties of sealants. Here, measurements performed at conditions as close as possible to those expected in-situ will yield more representative results. However, such measurements require relatively specialized and complex (i.e., expensive) equipment, and commonly take much longer to perform. The relative speed, ease and cost of simpler unconfined measurements make such methods preferable, especially when comparing many samples. However, where more accurate measurements are required (for example for numerical extrapolation beyond laboratory results), triaxial measurements carried out under in-situ conditions are strongly recommended. This is particularly necessary to support the improvement of current modelling capabilities.

Regardless of the test methods used, it is important to consider the parameters such as loading rate under which strength testing is performed. Due to the very low permeability of cements and other sealants, upon compressive loading, pore fluid pressures may increase, and this may cause early fracturing of the sample being tested. Standard loading rates (as prescribed in, e.g., [35]) do not always

take the very low permeabilities of novel sealants into account sufficiently, and may therefore lead to underestimation of the material properties (such as compressive strength) measured.

When assessing the impact of CO₂-exposure on the mechanical properties of a sealant sample, different reacted zones within the exposed sample will likely have different mechanical properties. If an exposed sample is tested to determine its overall mechanical properties, measurements will be strongly affected by these inhomogeneities and may not be representative at all. Fully reacting a sample such that a homogeneous material is obtained is usually not possible, or not practical. Alternative methods, such as micro-indentations (cf. [36]) may provide an effective tool for directly assessing changes in mechanical properties of differently-reacted zones in an exposed sealant sample, in particular when indentation depths are calibrated well with key mechanical properties such as compressive strength and Young's modulus. Therefore, such methods are recommended when trying to assess the impact of CO₂-exposure on sealant mechanical properties, especially when combined with sample-scale measurements (on homogeneous, i.e., unexposed, samples). (See also [15].)

5.3. Volumetric behaviour

Methods for measuring volumetric expansion or shrinkage during curing are presented in [37], and the use of these methods is recommended by documents such as [31, 32]. However, the method described is only performed at atmospheric pressure. While temperature is likely a more important variable determining the volumetric behaviour of a curing sealant, more accurately representing the in-situ environment with regards to pressure and fluid chemistry may also yield more representative measurements, and should be considered. Well sealant designers are primarily interested in the radial dimension change, whether shrinkage or expansion, typically tested per [37], but relevant, elevated pressures and temperatures.

5.4. Thermal properties

As noted in Deliverable 7.1 [15], standard methods exist to measure key thermal properties such as specific heat capacity, thermal conductivity, and thermal expansion coefficient (cf. [38]). While these methods typically measure such properties at atmospheric pressure, this is not expected to strongly impact obtained results. However, the degree of pore fluid saturation (i.e., free water content) in cementitious sealant samples does impact thermal properties such as thermal conductivity and specific heat capacity [39], and this should be taken into account when more accurate measurements are required, for example for numerical modelling.

5.5. Sample composition (mass/density; chemical/mineralogical composition; microstructure)

Compared to the material properties described above, the composition and microstructure of a hardened sealant, or of a hardened and exposed sealant, are relatively complex, and not measured as directly. However, changes in microstructure and mineral composition may be the clearest indicators of changes taking place in a sealant, and such changes may represent precursors to a loss of seal integrity.

Sample mass (and density) can be measured directly. When considering sample mass (or density), the main consideration is the sample water content of the sample, and whether to include that in the measurement. For wet samples, the surface-dry mass (obtained by wiping the surface of a sample with a moist cloth to remove excess water before quickly measuring the mass to limit evaporation) may be most reproducible. When a dry sample mass is needed, samples should be dried at a set temperature until no further loss of mass (due to evaporation) is observed. However, it should be noted that for many cementitious materials, drying may induce irrevocable microstructural changes due to drying-induced shrinkage of silica-gels and similar phases.

The bulk chemical composition of a sample may be determined using standard methods such as Inductively Coupled Plasma Optical Emission Spectroscopy (ICP-OES) after full digestion of the sample. Alternatively, it can be measured directly a solid sample using X-Ray Fluorescence (XRF), performing measurements on either a compressed powdered sample, or a representative cross-section through a solid sample. Note that while XRF may be faster, higher sensitivity and accuracy will be obtained through ICP-OES.

The mineralogical composition, and thus changes in sample mineralogy, can be obtained using X-Ray Diffraction (XRD). While, for example, Rietveld refinement will allow for the quantification of XRD-patterns, it should be kept in mind that the accuracy of such quantifications will be limited.

Changes in sample microstructure (due to changes in chemical and mineralogical composition) will likely result in local changes in density as well, that can readily be observed and quantified through X-Ray Computed Tomography (CT-scanning). The main benefits of CT-scanning are that it is a non-destructive technique that is relatively easy to perform, and that it can provide a full 3-dimensional image of the sample. However, the cost of the required equipment limits its availability. Furthermore, in practice, the spatial resolution of conventional CT-scanning (i.e., non-synchrotron radiation) is typically on the order of 10 μm /voxel, which may be too low to detect all changes in materials with very fine microstructures. Finally, where material alterations do not cause strong changes (or contrasts) in density, they are not observed using CT-scanning.

Scanning Electron Microscopy (SEM) can provide higher resolution imaging of sample microstructures. When combined with Energy Dispersive Spectroscopy (EDS), local chemical analyses can also be performed with a resolution down to $\sim 1 \mu\text{m}$. Furthermore, using SEM, changes in microstructure and mineralogy may be observed that were not visible using CT-scanning, and thus SEM may provide a better assessment of changes induced in a sealant through exposure. However, sample preparation for SEM analysis, as well as the analysis itself, can be time-consuming and requires skilled operators, making SEM (with EDS) relatively expensive. (See also [15].)

When assessing the impact of exposure (for example to CO_2 -containing fluids, or thermal shocks) on sample microstructure and composition, a wide array of analyses can be used, that vary in complexity and cost. The selection of analysis methods used in a specific study should depend on pre-existing knowledge or expectations, as well as the availability of equipment and the required accuracy of and confidence in the obtained results. When testing relatively unknown systems, such as fully new sealant systems under development, a more thorough investigation is likely required than when assessing relatively established materials.

5.6. Selection of testing methods.

A number of critical properties has been identified here, that are of key importance for ensuring long-term sealant integrity, or that should be considered to assess the impact of exposure of a sealant (for example to CO_2 -containing fluids). Next, testing methods have been discussed for these critical properties. When planning a study, for example developing a new sealant for an application such as geological CO_2 -storage or assessing and comparing different sealants for a specific application, a selection needs to be made what properties to focus on, and what testing methods to use to assess these properties.

When selecting what properties to focus on, the relevance of different properties needs to be considered (keeping in mind that for many of the critical properties listed in Table 2 testing is required by regulatory documents – see also [15]). Furthermore, when assessing the impact of exposure, it must be considered what properties are most likely to be affected strongest.

When selecting the methods to be used for measuring specific critical properties, the representativeness and accuracy of obtained measurements must typically be balanced against the complexity and equipment requirements, and thus cost, of various methods. For example, when quickly comparing a wider range of different candidate materials for a specific application, simpler

methods will often provide sufficient accuracy. On the other hand, a key challenge in assessing sealant integrity over the lifetime required for a CO₂-storage seal is extrapolation of obtained results well beyond the laboratory time (and length) scales. This is particularly true for relatively slow processes, such as the progress of sealant degradation, or the development of sub-critical damage (for example due to thermal cycles). One key means for improving the confidence with which such extrapolations of seal integrity can be made, is to select the most suitable testing methods and conditions for the relevant critical properties, in order to ensure high accuracy data are obtained as input for numerical models.

6. Sealant Assessment Table

Based on the key abilities and critical properties identified during the CEMENTTEGRITY project, as discussed in Deliverable 7.1 [15] and the current document, we have prepared a Sealant Assessment Table that can be used to assess and compare different sealants. The table contains individual sheets for the Key Abilities, and for the Critical Properties for sealants used in geological CO₂ storage. However, for future projects it can easily be expanded to accommodate further abilities or properties that are important to the project and application at hand. Colour coding (as suggested on the “Summary” sheet) may be used to easily visualise the performance of a sealant with regards to the different abilities and properties.

Fully filled-in Sealant Assessment Tables for the five CEMENTTEGRITY sealants have been attached to this report to demonstrate their use.

7. References

- [1] Alnes H, Eiken O, Nooner S, Sasagawa G, Stenvold T, Zumberge M. Results from Sleipner gravity monitoring: Updated density and temperature distribution of the CO₂ plume. *Energy Procedia*. 2011;4:5504-11.
- [2] Eiken O, Ringrose P, Hermanrud C, Nazarian B, Torp TA, Høier L. Lessons learned from 14 years of CCS operations: Sleipner, In Salah and Snøhvit. *Energy Procedia*. 2011;4:5541-8.
- [3] Yoo B-Y, Choi D-K, Kim HJ, Moon Y-S, Na H-S, Lee S-G. Development of CO₂ terminal and CO₂ carrier for future commercialized CCS market. *International Journal of Greenhouse Gas Control*. 2013;12:323-32.
- [4] Samara H, Al-Eryani M, Jaeger P. The role of supercritical carbon dioxide in modifying the phase and interfacial properties of multiphase systems relevant to combined EOR-CCS. *Fuel*. 2022;323:124271.
- [5] Celia MA, Bachu S, Nordbotten JM, Gasda SE, Dahle HK. Quantitative estimation of CO₂ leakage from geological storage: Analytical models, numerical models, and data needs. In: Rubin ES, Keith DW, Gilboy CF, Wilson M, Morris T, Gale J, et al., editors. *Greenhouse Gas Control Technologies 7*. Oxford: Elsevier Science Ltd; 2005. p. 663-71.
- [6] Carey JW, Wigand M, Chipera SJ, WoldeGabriel G, Pawar R, Lichtner PC, et al. Analysis and performance of oil well cement with 30 years of CO₂ exposure from the SACROC Unit, West Texas, USA. *International Journal of Greenhouse Gas Control*. 2007;1(1):75-85.
- [7] Duguid A, Scherer GW. Degradation of oilwell cement due to exposure to carbonated brine. *International Journal of Greenhouse Gas Control*. 2010;4(3):546-60.
- [8] Kutchko BG, Strazisar BR, Dzombak DA, Lowry GV, Thaulow N. Degradation of Well Cement by CO₂ under Geologic Sequestration Conditions. *Environmental Science & Technology*. 2007;41(13):4787-92.
- [9] Crow W, Brian Williams D, William Carey J, Celia M, Gasda S. Wellbore integrity analysis of a natural CO₂ producer. *Energy Procedia*. 2009;1(1):3561-9.
- [10] Kutchko BG, Strazisar BR, Lowry GV, Dzombak DA, Thaulow N. Rate of CO₂ Attack on Hydrated Class H Well Cement under Geologic Sequestration Conditions. *Environmental Science & Technology*. 2008;42(16):6237-42.
- [11] Liteanu E, Spiers CJ. Fracture healing and transport properties of wellbore cement in the presence of supercritical CO₂. *Chemical Geology*. 2011;281(3):195-210.
- [12] Zhang M, Talman S. Experimental Study of Well Cement Carbonation under Geological Storage Conditions. *Energy Procedia*. 2014;63:5813-21.
- [13] Wolterbeek TKT, Hangx SJT, Spiers CJ. Effect of CO₂-induced reactions on the mechanical behaviour of fractured wellbore cement. *Geomechanics for Energy and the Environment*. 2016;7:26-46.
- [14] Brunet J-PL, Li L, Karpyn ZT, Huerta NJ. Fracture opening or self-sealing: Critical residence time as a unifying parameter for cement–CO₂–brine interactions. *International Journal of Greenhouse Gas Control*. 2016;47:25-37.
- [15] van Noort R. Overview of current standards and common other testing methods used in wellbore sealant assessment. 2024 2024-01-26. Contract No.: CEMENTTEGRITY Deliverable 7.1.
- [16] van Noort R, Pluymakers A, Li K, Suryanto B, Starrs G. Development of Tailored Wellbore Sealants for CCS and Other Geological Storage Applications. *First Break*. 2024;42(9):89-94.
- [17] Kvassnes A, Clausen JA, Suryanto B, Kim J, inventors; RESTONE AS, assignee. Bond strength testing. USA patent US11054353B2. 2020.
- [18] Suryanto B, Starrs G, Kvassnes A, editors. Assessment of Bond Strength of Various Cementitious Sealants for CCS Well Applications. . *Proceedings of Joseph Aspdin 200 International Symposium, Innovations in Binder Technology*; 2024; Edinburgh.
- [19] van Noort R, Suryanto B, Starrs G, Lende G. Testing and developing improved wellbore sealants for CCS applications. *TCCS 12*; 19-21 June 2023; Trondheim, Norway.

- [20] Suryanto B, Starrs G. Interface integrity and properties of sealants after exposure to enhanced curing. CEMENTTEGRITY Concluding Seminar; 2024-11-27; Online.
- [21] Li K, Pluymakers A. Effects of Thermal Cycling on Wellbore Cement for CCS. CEMENTTEGRITY Concluding Seminar; 2024-11-27; online.
- [22] Li K, Friebel M, Pluymakers A. Thermo-mechanical Behaviour of the Sealant-steel Interface under Thermal Cycling for CCS. 2025 2025-02-01. Contract No.: CEMENTTEGRITY Deliverable 3.3.
- [23] Lende G. Forced-flow exposure of sealants to CO₂, and indentation mapping of carbonation extent. CEMENTTEGRITY Concluding Seminar; online.
- [24] van Noort R, Svenningsen G, Li K, Pluymakers A. Exposure of five cementitious sealant materials to wet supercritical CO₂ and CO₂-saturated water under simulated downhole conditions. International Journal of Greenhouse Gas Control. Submitted.
- [25] Mazurek M, Alt-Epping P, Bath A, Gimmi T, Niklaus Waber H, Buschaert S, et al. Natural tracer profiles across argillaceous formations. Applied Geochemistry. 2011;26(7):1035-64.
- [26] Bollermann T, Yuan T, Kulenkampff J, Stumpf T, Fischer C. Pore network and solute flux pattern analysis towards improved predictability of diffusive transport in argillaceous host rocks. Chemical Geology. 2022;606:120997.
- [27] Xiang Y, Al T, Scott L, Loomer D. Diffusive anisotropy in low-permeability Ordovician sedimentary rocks from the Michigan Basin in southwest Ontario. Journal of Contaminant Hydrology. 2013;155:31-45.
- [28] Brunet J-PL, Li L, Karpyn ZT, Kutchko BG, Strazisar B, Bromhal G. Dynamic Evolution of Cement Composition and Transport Properties under Conditions Relevant to Geological Carbon Sequestration. Energy & Fuels. 2013;27(8):4208-20.
- [29] van Noort R, Svenningsen G. Impact of CO₂ with impurities on integrity of wellbore cements during CCS. CEMENTTEGRITY Concluding Seminar; online.
- [30] Li K, Pluymakers AMH. Effects of thermal shocks on integrity of existing and newly-designed sealants for CCS applications. International Journal of Greenhouse Gas Control. 2024;133:104103.
- [31] NORSOK. D-010: Well integrity in drilling and well operations. NORSOK; 2021.
- [32] UK OG. Guidelines on Qualification of Materials for the Abandonment of Wells. Oil & Gas UK; 2015.
- [33] UK OE. Guidelines on Well Decommissioning for CO₂ Storage – Issue 1. Offshore Energies UK; 2022.
- [34] NOGEP. Industry Standard 45: Decommissioning of wells. NOGEP; 2021.
- [35] API. Recommended Practice 10B-2: Recommended Practice for Testing Well Cements.: American Petroleum Institute; 2013.
- [36] Lende G, Sørensen E, Jandhyala SRK, Van Noort R. State of the art Test Method to Quantify Progression Rate of Carbonation of Wellbore Sealing Materials. SPE Europe Energy Conference and Exhibition; 26-28 June 2024; Turin, Italy.
- [37] API. Recommended Practice 10B-5: Recommended Practice on Determination of Shrinkage and Expansion of Well Cement Formulations at Atmospheric Pressure. American Petroleum Institute; 2020.
- [38] ASTM. E228-22: Standard Test Method for Linear Thermal Expansion of Solid Materials With a Push-Rod Dilatometer. ASTM International; 2023.
- [39] Wolterbeek TKT, Hangx SJT. The thermal properties of set Portland cements – a literature review in the context of CO₂ injection well integrity. International Journal of Greenhouse Gas Control. 2023;126:103909.

8. Acknowledgement:

The CEMENTEGRITY project is funded through the ACT programme (Accelerating CCS Technologies, Horizon2020 Project No 691712).

Financial contributions from the Research Council of Norway (RCN), the Netherlands Enterprise Agency (RVO), the Department for Energy Security & Net Zero (DESNZ, UK), and Harbour Energy are gratefully acknowledged.

 Forskningsrådet

